ORIENTAL JOURNAL OF CHEMISTRY
An International Open Access, Peer Reviewed Research Journal
www.orientjchem.org
ISSN: 0970-020 X
CODEN: OJCHEG
2025, Vol. 41, No.(1):
Pg. 66-78

Evaluating the Applicability of Geopolymer Fly Ash as an Adsorbent for Phosphate Removal

RENU BALA[1], DINESH ARORA[2], ASHA SINGH[2], AZAD YADAV[2], RAJESH DHANKHAR[2] and SUNIL KUMAR CHHIKARA[1]*

[1]University Institute of Engineering & Technology, Maharshi Dayanand University, Rohtak (124001), Haryana, India.
[2]Department of Environmental Science, Maharshi Dayanand University, Rohtak (124001), Haryana, India.
*Corresponding author E-mail: renu.evs3012@gmail.com

http://dx.doi.org/10.13005/ojc/410107

(Received: July 06, 2024; Accepted: January 02, 2025)

ABSTRACT

Concerns of a critical nature have arisen in recent times regarding environmental challenges associated with phosphate and the depletion of resources by eutrophication. Recently, there has been research on geopolymer as environmentally friendly and cost-effective adsorbent, specifically targeting the removal of various pollutants in wastewater treatment. This investigation mainly focuses on solving challenges associated with the phosphate removal by employing Geopolymer Fly Ash (GPFA) as an adsorbent. GPFA was characterized using FESEM, EDX, FTIR and Zeta Potential. Batch experimentation was undertaken to evaluate the impact of different parameters including the initial phosphate ions concentration, pH level of the solution, contact time, temperature, and the quantity of adsorbent used. SEM imaging of GPFA revealed a granular structure with irregular pores structures. FTIR analysis identified specific functional groups on the adsorbent's surface, notably the presence of -OH groups, $-CH_2$ vibrations, and Si-O-Si vibrations. The optimal parameters for maximal phosphate removal, resulting in 95% removal rate using adsorbent amount of 0.25 g at a temperature of 298.15K with a pH value of 5.0. For the kinetics of phosphate sorption, the pseudo-second-order model delivered a good fit, while the adsorption isothermal data was well represented by the Freundlich model suggesting the adsorption process with multilayer coverage of adsorbent. In terms of thermodynamics, the adsorption of phosphate at the solid-liquid interface was determined to be exothermic and spontaneous. This research provides affordable and efficient material for cleaning wastewater, simultaneously suggesting a useful way to manage and use industrial solid waste.

Keywords: Geopolymer, Phosphate, Eutrophication, Isotherms, Thermodynamics.

INTRODUCTION

Phosphorus is a vital nutrient essential for the development of living organisms and the proper functioning of ecosystems.[1] But when the phosphorus concentration in a water body surpasses 0.03 ppm, it leads to accelerated growth of algae at an abnormal rate, oxygen depletion, which ultimately

degrades the water quality due to eutrophication.[2-4] Significant water pollution issues have been caused by the overuse of various chemical-based fertilizers, synthetic detergents, and different phosphorus compounds in residential and commercial properties and agriculture. This has led to the release of wastewater into the environment that contains different forms of phosphorus.[5-6]

Certain algae produce toxins harmful to both human health and wildlife. The disruption of aquatic ecosystems caused by these algal blooms can result in biodiversity loss and the deterioration of water quality, rendering it unfit for recreational activities and complicating the treatment of drinking water.[53] To reduce phosphate pollution, strategies like better nutrient management in agriculture, more advanced wastewater treatment techniques, tighter regulations on mining and agricultural practices, and increased public awareness are crucial. By tackling these pollution sources and encouraging sustainable practices, we can safeguard aquatic ecosystems and ensure the long-term sustainability of water resources for future generations.

Developing advanced phosphate removal technologies has become increasingly significant to meet more rigorous discharge necessities, as conventional methods comprising biological, chemical, and physical treatments, face challenges.[7] While biological degradation is widely available and effective, it struggles with eliminating trace levels of phosphate and maintaining strict operating conditions.[8] Chemical precipitation, on the other hand, requires high doses of metal salts and can lead to unavoidable secondary pollution.[9] Physical techniques like reverse osmosis and electrodialysis are known for their high energy consumption and poor selectivity[10]. Overall, Current water treatment techniques, such as chemical precipitation, membrane filtration, and electrochemical methods, face limitations including sludge generation, fouling, and high operational costs. In comparison, Adsorption is considered a favourable approach for the elimination of phosphates due to its quick and successful results, affordability, ease of use, and reusability.[11-13] Adsorbents offer several advantages, including high removal efficiency, reusability, and stable physicochemical properties in various conditions.[14] It also encounters challenges like low adsorption capacity, non-specific binding, material degradation, and economic viability concerns.

Current water treatment techniques, such as chemical precipitation, membrane filtration, and electrochemical methods, face limitations including sludge generation, fouling, and high operational costs. While adsorption is a promising alternative due to its effectiveness at low contaminant concentrations, it also encounters challenges like low adsorption capacity, non-specific binding, material degradation, and economic viability concerns. Additionally, environmental safety and regulatory issues surrounding advanced adsorbents further complicate their implementation. Overall, while each method has its drawbacks, advancements in material science may enhance the effectiveness of adsorption in future wastewater treatment applications.

Various low-cost treatment materials encompassing both natural and synthetic substances like bentonite, kaolinite, silicate, natural phosphate, activated carbon, aquatic weeds and geopolymer derived from fly ash, have proven effective in the successful confiscation of diverse pollutants found in water.[15-18] These materials have shown potential in addressing water pollution challenges effectively and economically. There is a marked inclination towards recycling waste materials to create useful and valuable resources. Coal fly ash, a significant waste material, poses considerable environmental and economic challenges when disposed of in large quantities.[16,20] An effective strategy for managing fly ash waste involves its conversion into geopolymer. This not only facilitates the removal of pollutants but also addresses the problem of ash accumulation as an industrial waste by-product.[21]

Fly ash-prepared geopolymer (GPFA) have many advantageous qualities that make them an excellent substitute for cement in terms of cost, environmental impact, and technological advantages.[22-23] Since the construction sector appears to be their primary use.[24] Geopolymer based on fly ash are also utilized for the sorption of harmful contaminants, heavy metals, and azo dyes.[25-27] The structural units of geopolymer are three-dimensional AlO_4-SiO_4 tetrahedra. They are amorphous aluminosilicates. They are produced using precursors that are aluminosilicate, specifically silicate minerals such as kaolin, fly ash, slag, and waste industrial materials.[28-29] Geopolymer are ring-like molecular chains and crystal-like structure which provide them remarkable adsorption capabilities for organic and inorganic contaminants, including heavy metals. Geopolymer are thought to be the best

low-cost adsorbents because of their remarkable adsorption abilities.[30]

According to the literature, only few researches have been done on the usage of fly ash-prepared geopolymer as an adsorbent material for the water treatment. This study looks into using GPFA as an adsorbent to eliminate phosphate contamination from synthetic solutions. The objectives of the study are (1) collection of fly ash and its transformation into geopolymer fly ash followed by its characterization (2) to examine the impacts of different parameters, which are pH, adsorbent dosage amount, initial phosphate ion concentration, interaction period and temperature on phosphate removal in the batch mode study; and (3) to assess the suitability of adsorption isotherms, kinetics, and thermodynamics.

MATERIALS AND METHODS

Preparation of Phosphate Stock solution

Throughout the experimental setup, pure chemicals of analytical grade were employed. The phosphate stock solution of 1000 ppm was prepared utilizing Potassium Dihydrogen Phosphate (KH_2PO_4) and afterwards standards were prepared from the main stock solution.

Procedure for the synthesis of Geopolymer fly ash adsorbent

Collection of fly ash was done from the coal-fired thermal power station located at 29°23°50°N and 76°52°52°E near Khukhrana, Panipat, Haryana. The fly ash was first sieved and washed away 3-4 times with deionized water. Later, it was dried in oven at 100°C for 24 h and further finely into a powder. To synthesize fly ash-based geopolymer, a mixture was prepared by combining 6 g of fly ash with 7.2 g of solid NaOH, and the resultant blend was finely ground into a powder. This powder was then heated to 600°C in muffle furnace for 2 hours. Following the NaOH fusion treatment, the resulting solids were ground into a fine powder, and then 60 mL of distilled water was mixed to it. This mixture was then heated to 80°C for approximately 75 h while being agitated at 400 rpm. The slurry was subsequently placed into an autoclave lined with Teflon and heated to 120°C for two hours. The resulting sample was strained, subjected to several washing cycles with deionized water until it attained a neutral pH (pH<7), and lastly, oven-dried at 100°C for 24 hours. The dried material was stored in hermetic containers for later use in phosphate adsorption.[31]

Identification of adsorbent

The external morphology of GPFA was examined using FESEM-EDX (JEOL 7610F Plus), while functional groups responsible for phosphate adsorption were identified using an FTIR spectrophotometer (Bruker Alpha) in the wavelength range of 500–3500 cm^{-1} before and after the adsorption process.

Batch experiments

The phosphate stock solution (1000 mg/L) was prepared by dissolving a sufficient quantity of potassium dihydrogen phosphate (KH_2PO_4) in deionized water. From this main stock solution, standard solutions of varying concentrations were prepared. Batch experimentations were conducted using 50 mL of KH_2PO_4 solution in 100 mL conical containers. To adjust the solution's pH before introducing the adsorbent, 1N HCl and 1N NaOH solutions were utilized. The batch experiments involved assessing the impact of pH, amount of adsorbent dosage, initial phosphate concentration, interaction period, and temperature.[32] The experimentations were conducted in triplicate sets, covered a pH ranging 2 to 9 for the phosphate solution, adsorbent doses from 0.05 to 0.5 g for GPFA, initial ion concentrations from 20 to 160 ppm for phosphate ions, contact times varying from 15 to 120 min and temperatures ranging from 5 to 45°C. For pH optimization, conical containers having 0.2 g adsorbent dose and 50 mL of phosphate solution were incubated in a shaker at 25°C temperature with agitation speed of 100 rpm for 1 hour. Whatman filter paper was utilized to separate the adsorbent after incubation. The phosphate determination was done using stannous chloride method. In 50 mL of phosphate solution, firstly a single drop of phenolphthalein indicator was dropped and then stirred after that 4 mL of the ammonium molybadate was added to it and mix thoroughly, and later on 0.5 mL of stannous chloride was introduced to the solution and mixed well. After allowing the blue colour to develop, the phosphate concentration was measured. Phosphate ion concentration in synthetic solution was determined using UV-1800 Shimazu at a wavelength of 690 nm. The intensity of the blue color is directly proportional to the sample's phosphate concentration.[33] The adsorption capacity (q_e), representing the amount of adsorbed phosphate ions per unit amount

of adsorbent at equilibrium was determined by applying Eq. (1).

$$\text{Uptake capacity } (q_e) = \frac{C_i - C_e}{m} * V \quad (1)$$

Where in q_e depicts the quantity of phosphate ion adsorbed at equilibrium (mg/g), C_i and C_e depicts the beginning and final concentration of phosphate ions (ppm), V depicts the capacity of phosphate solution (L), m depicts quantity of adsorbent (g).

Removal efficiency (%) for phosphate ion was computed with the help of Eq. (2) as follows:

$$\text{Removal efficiency } (\%) = \frac{C_i - C_e}{C_i} * 100 \quad (2)$$

Where C_i and C_e depict the beginning and final concentrations of phosphate ion (ppm).

Isotherms, kinetics and thermodynamics studies

Various isotherm models such as "Langmuir, Freundlich, and Temkin", were used to examine the adsorption of phosphate onto GPFA. "Lagergren's pseudo-first-order" and "pseudo-second-order" equations were employed to predict the kinetics process of the adsorption. Thermodynamic equations were utilized to assess factors for instance "enthalpy change (ΔH°)," "entropy change (ΔS°)," and "free energy change (ΔG°)" associated with the phosphate adsorption onto GPFA.

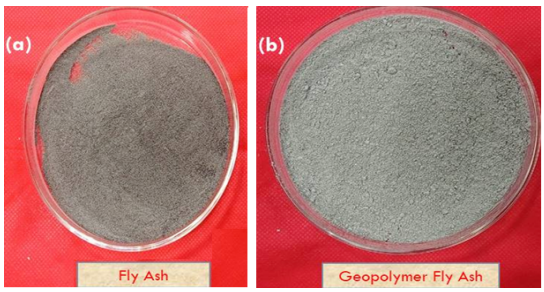

Fig. 1(a) Raw Fly Ash (b) Synthesized Geopolymer Fly Ash

RESULTS AND DISCUSSION

Identification of adsorbent

SEM Interpretation

The SEM images of GPFA pre and post phosphate adsorption have been presented in Fig. 2a and Fig 2b). The images show that before adsorption the surface of adsorbent has irregular, spherical and porous structures which are macro porous, meso-porous and micro porous in nature. However, after adsorption the granular structure of GPFA indicates the agglomeration of phosphate ions on GPFA surface which potentially showed the changes in microstructure of adsorbent.

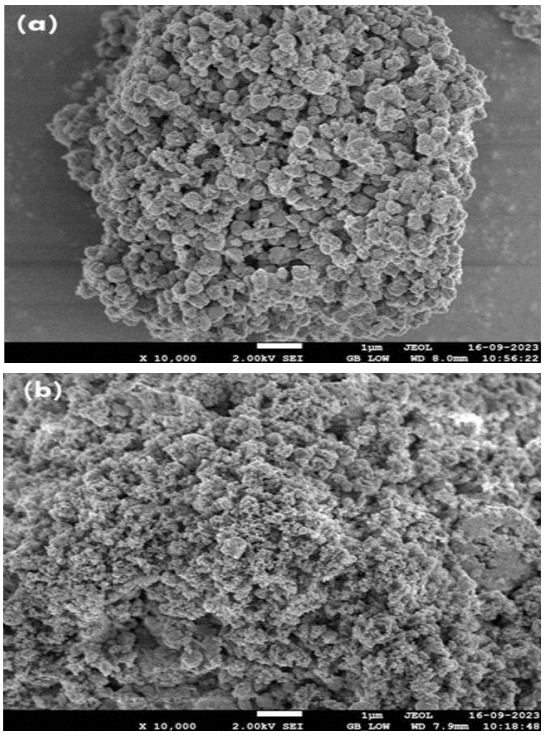

Fig. 2. SEM imageries of GPFA (a) before adsorption (b) after adsorption

EDX interpretation

EDX (Energy-Dispersive X-ray spectroscopy) is a technique used to detect and quantify the elements present in a material. Fig. 3 represents the elemental composition of GPFA adsorbent after adsorption of phosphate. The image displays the peaks corresponding to different elements existing in the adsorbent. The points of Carbon (C), Oxygen (O), Aluminium (Al) Silica (Si), Sodium (Na) and Potassium (K) and their relative weight% obtained were 15.5, 50.2, 9.6, 12.7, 5.3 and 5.3 respectively for GPFA have been noticed.

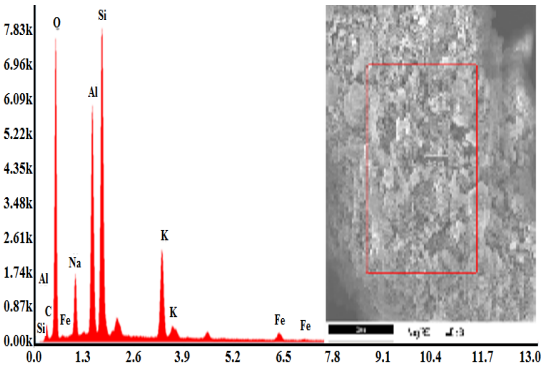

Fig. 3. EDX analysis of GPFA

FTIR interpretation

Figure 4 presents the outcomes of the FTIR analysis for GPFA. Peaks were identified within the wavenumber ranging from value of 500 to 3500 cm^{-1}. The noteworthy maxima were perceived at around 2963.01, 2878.86, 2664.96, 1000.00, 674.46 cm^{-1} respectively for GPFA (Fig. 4a). The PO_4^{3-} ion-free spectra of GPFA displays maxima at 3342.81, 3218.38, 3060.10, 2921.00, 2849.88, 2355.24, 1540.02, 1001.013, 719.17 (Fig. 4b) representing –OH stretching, C-H and $–CH_2$ stretching, deformation of HCO_3- ions due to infrared bands, N-H stretching and broad peak at 1000 indicates Si-O-Si vibration due to geopolymerization. After phosphate adsorption, it was revealed that FTIR peaks increased in numbers, and developed other minor peaks indicating that phosphate significantly enhances the functional group count on over the adsorbent surface.

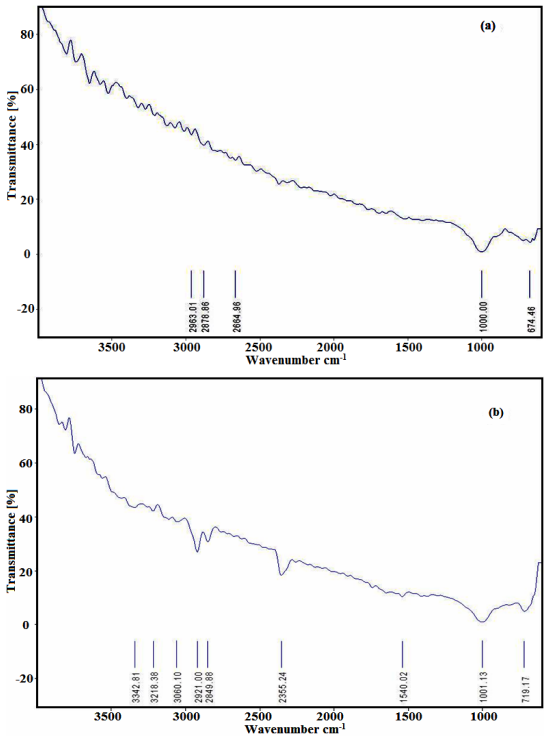

Fig. 4. FTIR spectrums of (a) GPFA pre adsorption (b) GPFA post adsorption

Zeta Potential of Geopolymer fly ash

Zeta Potential (ζ-potential) refers to the electrical potential difference among the bulk of the dispersion medium and the stationary layer of liquid attached to the surface of a dispersed particle. It signifies the electrical charge that forms at the interface where a solid surface contacts its surrounding liquid environment. In colloid chemistry, Zeta potential values ranging between -30 mV and +30 mV signify a high degree of stability in colloidal dispersions. The zeta potential detected for the geopolymer fly ash was –35.6 mV, indicating high stability of the synthesized adsorbent (Figure 5).

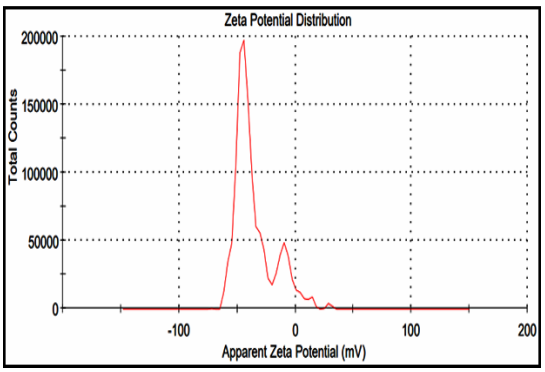

Fig. 5. Zeta potential curve for Geopolymer fly ash

Zeta size of geopolymer fly ash

The zeta size analysis for geopolymer fly ash (GPFA) is shown in Fig. 6. Using a zeta sizer, which measures particle sizes from nanometres to micrometres, it was found that GPFA has a hydrodynamic size of 190 nm, indicated by a single peak.

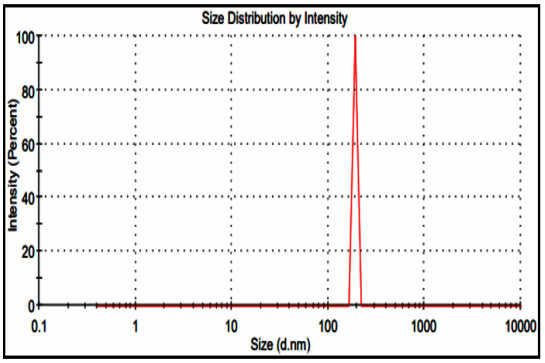

Fig. 6. Zeta size of Geopolymer fly ash

Optimization of various parameters for adsorption process

Influence of pH

Phosphate ion removal is significantly influenced by pH. Batch experiments were performed by changing the pH ranging from 2 to 9, with a fixed adsorbent mass of 0.2 g for geopolymer fly ash. Other parameters, including 20 ppm initial phosphate concentration, 1 h of interaction time and temperature of 25°C were held persistent. The impact of pH on the exclusion of phosphate ions by GPFA is illustrated in Fig. 7. Outcomes indicated

that the adsorbent achieved maximum phosphate removal at pH 5.0, with the adsorption removal (%) declining as the pH increased. An alike trend was observed in the case of uptake capacity. The phosphate ion predominately exists as H_3PO_4 at acidic pH levels as it got easily absorbed onto GPFA due to favourable electrostatic attraction. As the pH upsurges, it undergoes a conversion into other forms of phosphorous ions, including H_2PO_4-, HPO_4^{2-} and PO_4^{3-} which face repulsion from the increasingly negatively charged surface of GPFA, resulting in reduced adsorption efficiency. A decline in phosphate adsorption with a rise in pH may be ascribed to the interaction among two anions, specifically HPO_4^{2-} and OH- ions, adsorbed over the adsorbent's surface which is governed by OH- ions.[34]

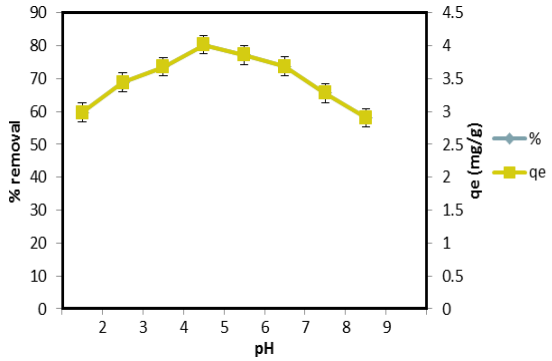

Fig. 7. Influence of pH by GPFA on adsorption of phosphate

Influence of adsorbent dose

In the batch experiments, various dosages of GPFA varying from 0.05 to 0.5 g were tested with a 20 ppm phosphate solution at pH 5.0, a 1 h of contact period, 100 rpm stirring rate, and a temperature of 25°C to evaluate the removal of phosphate ions. The impact of dosage on phosphate removal and the corresponding uptake capacity at different doses is shown in Fig. 8. It was noticed that the removal percentage of phosphate upsurged as the dosage of GPFA was raised, eventually reaching a saturation point. Simultaneously, the uptake capacity (q_e) declined as the adsorbent dose upsurged. This phenomenon can be clarified by the fact that as the adsorbent dose increased, more active binding sites on the adsorbent became available for phosphate adsorption on GPFA. However, the adsorption capability declined due to decrease in number of phosphate ions in solution with increase of adsorbent dose.[35] The phosphate removal efficiency for GPFA reached 95.55% at a dose of 0.25 g. A similar study conducted on phosphate adsorption using a zeolite/geopolymer composite.[36]

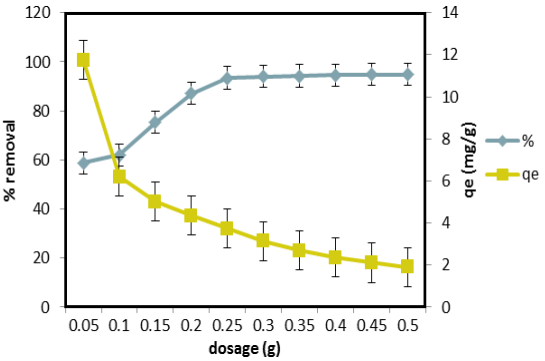

Fig. 8. Influence of adsorbent dosage by GPFA on phosphate adsorption

Influence of initial ion concentration

The effect of initial ion concentration was studied through a series of batch experimentations where the phosphate solution concentration ranged from 20 to 160 ppm. These experiments were conducted using the optimized dose of the adsorbent, a pH of 5.0, contact period of 60 min at a temperature of 25°C. The outcomes illustrating the effect of initial concentration on phosphate removal by GPFA are represented in Fig. 9. It was noticed that the adsorption efficiency was maximum at an initial concentration of 20 ppm and subsequently declined with upsurge of phosphate concentration in the solution. This decline in efficiency can be attributed to the fullness of adsorption sites on the adsorbent material at elevated ionic concentrations.[37] At lower concentrations, there are more available adsorption sites, promoting faster binding on phosphate ions. However, at larger concentrations, intra-particle diffusion forces the adsorbate to disperse across the entire surface of the adsorbent.[38] The most effective sorption efficiency was achieved at 20 ppm of concentration. Conversely, the uptake capacity (q_e) raises as the phosphate concentration in the solution rises because greater number of active sites for binding become accessible for sorption. The existence of phosphate ions within the solution serves as a crucial driving force in overcoming the mass transfer resistance between the adsorbent and the adsorbate.[39]

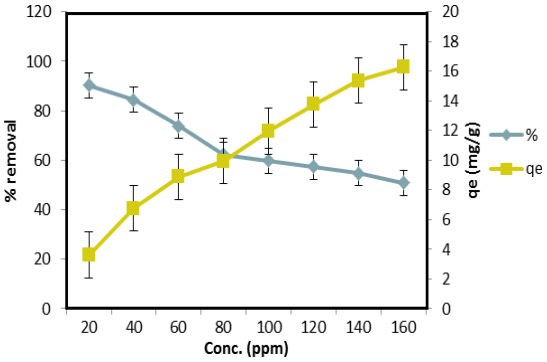

Fig. 9 Influence of initial phosphate ion concentration by GPFA on phosphate adsorption

Influence of contact time

Phosphate removal is significantly impacted by the contact period of the adsorption process. The impact of time on the removal of phosphate ions using GPFA is illustrated in Fig.10. Experiments were conducted with different interaction times, ranging from 15 min to 120 min, while maintaining a pH of 5.0 and phosphate concentration of 20 ppm at 25°C. The outcomes demonstrated that as the contact period was extended from 15 to 90 min, both the adsorption rate and the uptake capacity (q_e) for phosphate ions increased. This rapid phase occurs due to the strong concentration gradient and the full availability of binding sites on the adsorbent. However, beyond 90 min, No discernible rise in adsorption was seen. This observation suggests that the adsorbent material has a finite number of active binding sites for adsorption, and these sites become saturated over time.[40] Similar findings were reported in a study that utilized magnetic oxide nanoparticles loaded with tea waste for phosphate remediation.[41]

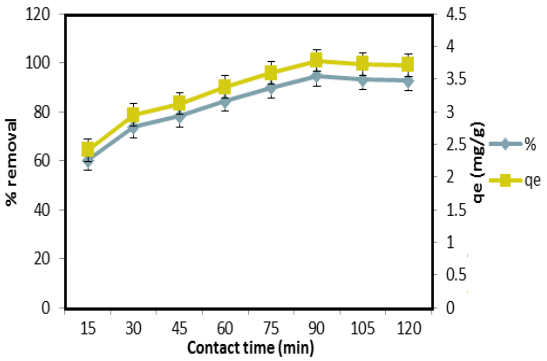

Fig. 10 Influence of contact period by GPFA on phosphate adsorption

Influence of Temperature

Temperature is a crucial factor in the process of adsorption. To investigate its influence, experimental studies were executed at various temperatures varying from 5 to 45°C, using the optimized dose of GPFA, pH 5.0, for a period of 90 min with 20 ppm of phosphate ion concentration. The influence of temperature on phosphate sorption by GPFA is illustrated in Fig. 11. The outcomes indicated that both the removal percentage and uptake capacity (q_e) upsurged as the temperature increased, but this trend reversed after reaching 15°C. The rise in temperature results in increased thermal energy within the system, which, in turn, enhances the mobility of phosphate ions. This increased mobility promotes desorption, leading to a reduction in overall adsorption. Similar findings have been reported in earlier research studies conducted by different researchers.[40,42]

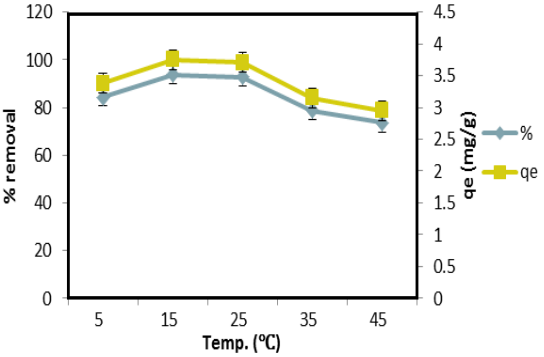

Fig. 11. Influence of temperature by GPFA on phosphate adsorption

Isotherms, kinetics, and thermodynamics studies

Understanding adsorption isotherms and kinetics is essential for the practical application of adsorption processes in water treatment, environmental remediation, and industrial processes. These models provide insights into how an adsorbent behaves under different conditions, enabling optimization of adsorption systems for efficiency and cost-effectiveness.

Adsorption isotherms

The research focused on examining the equilibrium association between the GPFA (adsorbent) and phosphate ions (adsorbate) in the solution employing three diverse isothermal models: Langmuir, Freundlich, and Temkin isotherm. The isothermal studies involved adjusting the adsorbent

dosage under specific conditions, including a pH value of 5.0, an initial phosphate concentration of 20 ppm, a contact period of 1 h at a temperature of 25°C.

Langmuir isotherm

The Langmuir isotherm, established on kinetic principles, is an empirical model that deposits zero accumulation at equilibrium due to equal rates of adsorption and desorption on the surface.[43] (Langmuir, 1916). This isotherm is founded on several assumptions, including (a) homogeneous sites on the adsorbent surface, (b) monolayer adsorption, (c) constant adsorption energy, and (d) the absence of lateral molecular interaction. The linearlized form of Langmuir isotherm was used to examine the maximum uptake capacity, which is shown in Eq. (3)

$$\frac{C_e}{q_e} = \frac{1}{bq_m} + \frac{C_e}{q_m} \quad (3)$$

The Langmuir isotherm model for phosphate ions is validated by a linear plot between C_e/q_e and C_e. Where C_e represents the final concentration of adsorbate (ppm), b represents the Langmuir constant, and q_e indicates the maximum uptake capacity (mg/g). These constants values can be found by analysing the slope and intercept of the linear plot of the experimental data of C_e/q_e vs. C_e.

Langmuir's description of the fundamental characteristics of the isotherm led to the calculation of a dimensionless constant known as the separation factor (R_L).

Separation Factor

$$R_L = \frac{1}{(1+bC_i)} \quad (4)$$

Where R_L depicts a limitless identity well-known as separation factor attained from langmuir, b depicts Langmuir constant and C_i depicts the initial phosphate ion concentration. The dimensionless separation factor (R_L) holds four significant implications varied from 0 to 1. An adsorbate and adsorbent are interacting successfully and efficiently when the value of $0<R_L<1$ indicates a favorable isotherm. On the other hand, $R_L>1$ represents an unfavorable isotherm; $R_L=0$ represents an irreversible isotherm; and $R_L=1$ represents a linear isotherm.

From Fig. 12 and Table 1 the value of R^2 was 0.65 for the adsorbent. Separation factor (R_L) calculated using Eq. (4) yielded a value of 0.19 for GPFA. This value indicates that the adsorption approach is both feasible and effective, falling within the acceptable range of $0<R_L<1$.[44]

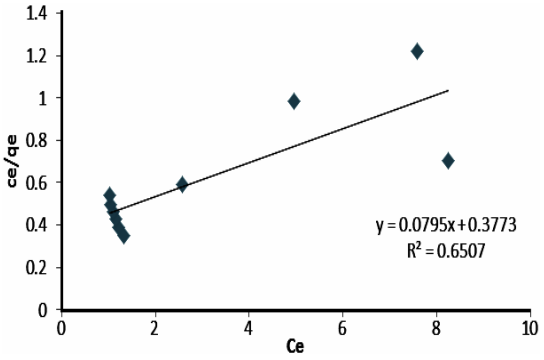

Fig. 12 Langmuir isotherm plot for phosphate adsorption on GPFA

Table 1: Parameters of the isotherm model for phosphate adsorption onto GPFA

Isothermal model	Parameters	GPFA
Langmuir	q_m (mg/g)	12.57
	B	0.21
	R^2	0.65
	R_L	0.19
Freundlich	N	1.65
	K_f (L/g)	2.354
	R^2	0.85
Temkin	B_T (KJ/mol)	8.32
	A_T (g/L)	1.99
	R^2	0.74

Freundlich Isotherm

In the Freundlich isotherm, the adsorption process involves molecules binding to heterogeneous surfaces, resulting in the formation of multiple layers. Additionally, interactions occur between the molecules that have been adsorbed.[45] The equation provided below gives the Freundlich model's linear form:

$$\log q_e = \log K_f + 1/n \log C_e \quad (5)$$

Where C_e depicts the equilibrium concentration (ppm), q_e depicts the equilibrium phosphate ion adsorbed quantity (mg/g), K_f stands for the adsorption capacity, n for

adsorption intensity. Plotting the intercepts and slopes of the curve between log C_e and log q_e allows for the calculation of K_f and n. It was observed from Fig. 13 and Table 1. showed that the value of correlation coefficient was 0.85 for GPFA respectively. Thereby, it was concluded that Freundlich isotherm was well fitted as contrary to Langmuir isotherm revealing the heterogeneous surface of adsorbent.

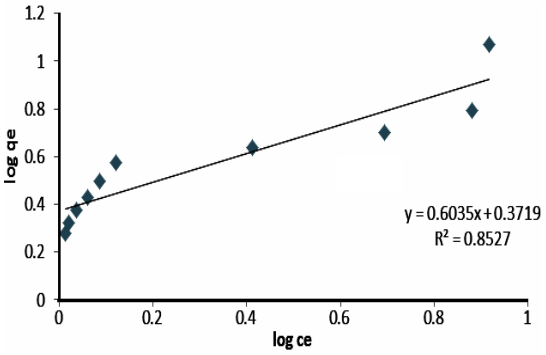

Fig. 13. Freundlich isotherm plot for phosphate adsorption on GPFA

Temkin Isotherm

The Temkin model reflects on interactions among the adsorbent and the adsorbate and deals with multilayer adsorption process.[46] However, it neglects very minor and very large concentration values.[47] This model is employed to characterize the adsorption behaviour but it is not appropriate for extremely low or high concentrations of the adsorbate. The Temkin isotherm model postulates that the decrease in the heat of adsorption with temperature follows a linear trend, as opposed to a logarithmic one. It can be expressed as:

$$q_e = \frac{R_T}{B_T} lnA_T + \frac{R_T}{B_T} lnC_e \quad (6)$$

Where, q_e is the equilibrium remaining quantity of phosphate ion adsorbed on GPFA (mg/g), C_e depicts equilibrium phosphate ion concentration (ppm), T depicts the absolute temperature (K), and R depicts universally accepted gas constant (8.314J/mol/K). Temkin's constants, B_T (J/mol) and A_T (g/L) relate to the heat of adsorption and the Temkin isotherm constant, respectively. For GPFA, the Temkin plot was drawn among qe against ln C_e, as seen in Fig. 14. B_T and A_T values can be calculated using the slope and intercept, respectively.

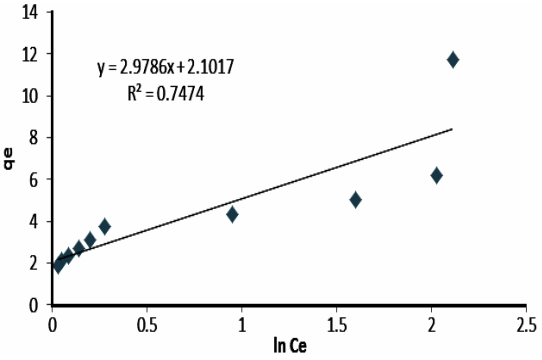

Fig. 14. Temkin isotherm plot for phosphate adsorption on GPFA

Adsorption kinetics

The kinetic studies involved adjusting the contact times under specific conditions, including a pH value of 5.0, an initial phosphate concentration of 20 ppm, adsorbent dose of 0.25 g and temperature of 25°C. To ascertain the adsorption rate, various kinetic models, involving “Lagergren’s pseudo-first-order,” “pseudo-second-order,” and “intra-particle diffusion” models, were examined using the adsorption data.

Pseudo-first-order Model

The "pseudo-first-order kinetic equation of the Lagergren model" describes a relationship where unoccupied adsorption sites have a direct influence on the rate of adsorption.[48] This model is frequently used when the adsorption process is mainly driven by physical interactions, like Van der Waals forces, rather than by chemical bonding. The linearized form of PFO is typically conveyed as follows:

$$\text{Log}\,(q_e - q_t) = \log q_e - \frac{k_1 t}{2.303} \quad (7)$$

Where K_1 is the PFO rate constant (1/min) and q_e and q_t stand for the quantity of phosphate ions adsorbed per unit mass of GPFA (mg/g) at equilibrium and at time (t).

A kinetic plot for the pseudo-first-order kinetic curve was generated by plotting log (q_e-q_t) and t as depicted in Fig. 15. The slopes and intercepts were then used to derive the K_1 and q_e values, respectively. The correlation coefficient obtained from Fig. 15 for GPFA was 0.64. The correlation coefficient exceeding 0.9, suggests a strong arrangement among the adsorption data values.

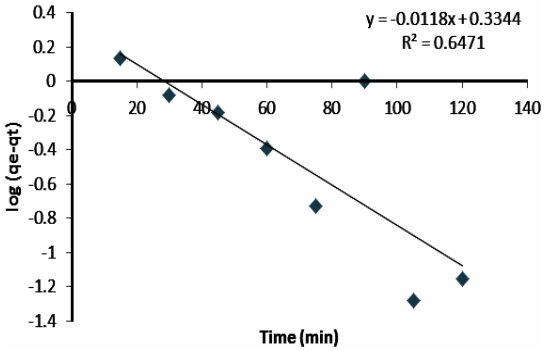

Fig. 15. Pseudo-first-order kinetic plot for phosphate adsorption on GPFA

Pseudo-second-order Model

This model presumes that the adsorption process is mainly driven by chemical interactions, such as covalent or ionic bonding. The adsorption rate is influenced by the square of the total number of vacant sites, according to the pseudo-second-order equation.[49] The pseudo-second-order equation in linearized form can be elucidated as follows:

$$\frac{t}{q_t} = \frac{1}{k_2 q_e 2} + \frac{1}{q_e} \quad (8)$$

Where, K_2 represents the PSO rate constant (g/mg/min) and qe and qt are the quantities of phosphate ions adsorbed onto GPFA (mg/g) at equilibrium at time (t).

Figure 16 displays a pseudo-second order plot that was generated among t/q_t and t. The values of q_e and K_2 were determined by using the slope and intercept of the curve between t/q_t and t. The obtained R^2 value for the adsorbent was 0.997. It was evident from Table 2 that The pseudo-second-order model performed better in fitting the adsorption data because strong agreement was found among estimated q_e and experimental q_{exp} and R^2 values were also closer to unity than those of the pseudo-first-order model.

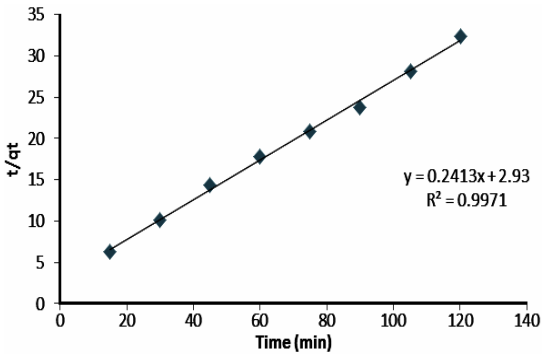

Fig. 16. Pseudo-second-order plot for phosphate adsorption on GPFA

Table 2: Parameters of the kinetic model for phosphate adsorption onto GPFA

Kinetic model	Parameters	GPFA
Experimental adsorption capacity	q_{exp} (mg/g)	3.68
Pseudo-first-order kinetics	q_e (mg/g)	1.02
	K_1 (1/min)	0.77
	R^2	0.64
Pseudo-second-order kinetics	q_e (mg/g)	4.14
	K^2 (g/mg/min)	0.019
	R^2	0.997
Intra-particle diffusion	K_i (mg/g $min^{0.5}$)	0.19
	x_i (mg/g)	1.83
	R^2	0.92

Intra-particle diffusion

The intra-particle uptake in the adsorption process and pore diffusion serve as the foundation for the intra-particle diffusion concept. Intra-particle diffusion is a key step in determining the overall rate of adsorption, especially when the adsorbent has a significant porous structure. To ascertain the diffusion procedure, [50]Weber and Morris (1963) observed that intra-particle diffusion of the adsorbate exhibits a direct proportionality alongwith the square root of time during adsorption and is represented in linearized form:

$$q_t = k_i \sqrt{t} + x_i \quad (9)$$

Where k_i represents the intra-particle diffusion rate constant (mg/g $min^{0.5}$) and x_i is the border layer's wideness (mg/g). The x_i and k_i values were estimated based on from the intercepts and slopes of qt against √t plot. (Fig. 17). The values of k_i and x_i are 0.19 and 1.83 with the correlation coefficient of 0.92 for the adsorbent respectively (Table 2).

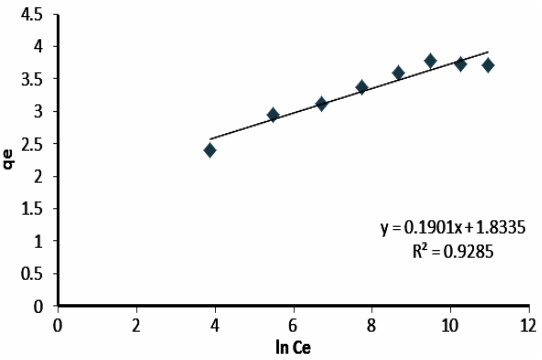

Fig. 17. Intra particle diffusion for phosphate adsorption on GPFA

Thermodynamic study for phosphate adsorption on GPFA

Thermodynamic parameters such as "enthalpy (ΔH°)," "free Gibbs energy (ΔG°)," as well as "entropy (ΔS°)" fluctuations affect the spontaneous nature of the adsorption process. A decline in ΔG° indicates the spontaneous nature of the adsorption process, especially as the temperature decreases.[51] This study examined thermodynamic parameters across various temperatures, ranging from 278.15 K with a constant interval of 10 K up to 318.15 K. The determination of thermodynamic parameters was conducted using the following equations:

$$lnK_d = \frac{\Delta S°}{R} - \frac{\Delta H°}{RT} \quad (10)$$

$$\Delta G° = \Delta H° - T\Delta S° \quad (11)$$

K_d, which is calculated as q_e/C_e, is a constant representing the equilibrium state. Here, q_e denotes the phosphate equilibrium uptake capacity (mg/g), while C_e stands for the final concentration of phosphate ions (ppm). T represents temperature (K), and R depicts widely recognized gas constant (8.314 J/mol/K). In Fig. 18, the slope and intercept of the Van't Hoff plot (lnK_d vs. 1000/T) were used to calculate thermodynamic parameters such as ΔH° (kJ/mol) and ΔS° (kJ/mol/K).

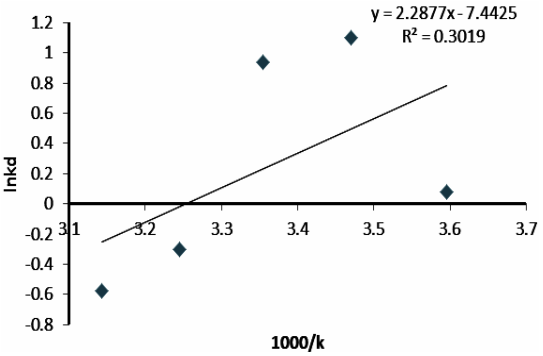

Fig. 18. Thermodynamics plot for phosphate adsorption on GPFA

The thermodynamic study outcomes for GPFA are outlined in Table 3. Across temperatures varying from 278.15 K to 308.15 K, ΔG° for GPFA exhibited a range from -2.04 to -0.22 KJ/mol, signifying a spontaneous adsorption process. However, at 318.15 K, ΔG° recorded a value of 0.39, indicative of a non-spontaneous behaviour in the adsorption process. The below zero values of ΔH° suggest an exothermic sorption process, while the positive value of ΔS° imply an expansion of randomness at the solid-liquid interface.

Table 3: Thermodynamic analysis of variables for phosphate adsorption onto GPFA

Adsorbent	ΔH°(kJ/mol)	ΔS°(KJ/K. mol)	ΔG°(KJ/mol)				
			278.15 K	288.15K	298.15K	308.15K	318.15K
GPFA	-19.01	0.061	-2.04	-1.44	-0.83	-0.22	0.39

Comparison of various adsorbents with GPFA for phosphate adsorption

Table 4 analyse and compare the maximal sorption capacities of various types of adsorbents for adsorption of phosphate. Various adsorbents such as red mud[54], lithium intercalated gibbsite[55], bark carbon[56] and dewatered alum sludge[57] been used for confiscation of phosphate from synthetic solutions.

Table 4: Comparison of GPFA with other adsorbents

Adsorbent	Adsorption capacity	pH	Temperature (°C)	References
Red mud	0.6	4.0	25	54
Lithium intercalated gibbsite	0.3	5.0	25	55
Bark carbon	1.79	7.0	30	56
Dewatered alum sludge	3.5	4.13	25	57
GPFA	4.14	5.0	25	This study

CONCLUSION

The geopolymer fly ash was evaluated for the phosphate adsorption from synthetic solutions. The batch experiment was conducted to identify the influence of different parameters. The optimal elimination was noticed at pH 5.0 alongwith initial concentration of 20 ppm in 90 min at 15°C with sufficient agitation. SEM analysis showed the porous and granular structure with irregular pore spaces. FTIR interpretations tell about the availability of hydroxyl ions, Si-O-Si vibrations on the adsorbent surface. The adsorption data exhibited the strong co-relation with the Freundlich

isotherm model revealing multilayer adsorption with heterogeneous surface. The pseudo-second-order model was found to be well suited rather than pseudo-first-order model. Thermodynamics study revealed adsorption process was exothermal and spontaneous in nature. Hence, fly ash is a readily available and plentiful adsorbent that can be easily converted into a geopolymer. Overall, GPFA presents a highly effective and sustainable solution for phosphate removal from wastewater, particularly in secondary treatment plants. Its high surface area and porous structure facilitate multilayer adsorption, enhancing its capacity to bind phosphate ions. As a low-cost and non-toxic adsorbent derived from industrial by-products, GPFA not only reduces economic burdens but also promotes environmentally friendly practices. Its adaptability to various conditions, coupled with potential modifications to improve performance, positions GPFA as a versatile option for addressing multiple contaminants in wastewater. Ultimately, the use of GPFA contributes significantly to mitigating eutrophication in surface waters while supporting broader water treatment strategies and waste valorization efforts. Nevertheless, to make this method suitable for real-world applications, additional column adsorption experiments in a continuous flow system are necessary. These experiments will help fine-tune the process parameters and scale up the approach for field applications.

ACKNOWLEDGEMENT

The author acknowledges the Department of Environmental Science, Maharshi Dayanand University, Rohtak for providing research facilities.

Conflict of interest

No potential conflict of interest was reported by the author(s).

REFERENCES

1. Li, B.; Dong, S. L.; Huang, Y. F.; Li, P.; Yu, W.; Wang, G. Q.; Young, B., *Journal of Cleaner Production*., **2021**, *279*, 123441.
2. Li, G.; Gao, S.; Zhang, G.; Zhang, X., *Chemical Engineering J*., **2014**, *235*, 124-131.
3. Awual, M. R., *Journal of Cleaner Production*., **2019**, *228*, 1311-1319.
4. Park, J. H.; Hwang, S. W.; Lee, S. L.; Lee, J. H.; Seo, D. C., *Applied Biological Chemistry*., **2021**, *64*(1), 1-9.
5. Wu, B.; Wan, J.; Zhang, Y.; Pan, B.; Lo, I. M., *Environmental Science & Technology*., **2019**, *54*(1), 50-66.
6. Yang, Y.; Koh, K. Y.; Li, R.; Zhang, H.; Yan, Y.; Chen, J. P., *Journal of Hazardous Materials*., **2020**, *392*, 121952.
7. Pap, S.; Kirk, C.; Bremner, B.; Sekulic, M. T.; Shearer, L.; Gibb, S. W.; Taggart, M. A., *Water Research*., **2020**, *173*, 115573.
8. Bacelo, H.; Pintor, A. M.; Santos, S. C.; Boaventura, R. A.; Botelho, C. M., *Chemical Engineering Journal*., **2020**, *381*, 122566.
9. Recepoglu, Y. K.; Goren, A. Y.; Orooji, Y.; Khataee, A., *Chemosphere*., **2022**, *287*, 132177.
10. Almanassra, I. W.; Kochkodan, V.; Mckay, G.; Atieh, M. A.; Al-Ansari, T., *J. Environmental Management*., **2021**, *287*, 112245.
11. Lalley, J.; Han, C.; Li, X.; Dionysiou, D. D.; Nadagouda, M. N., *Chemical Engineering Journal*., **2016**, *284*, 1386-1396.
12. Feng, L.; Zhang, Q.; Ji, F.; Jiang, L.; Liu, C.; Shen, Q.; Liu, Q., *Chemical Engineering Journal*., **2022**, *430*, 132754.
13. Mohammadi, R.; Hezarjaribi, M.; Ramasamy, D. L.; Sillanpää, M.; Pihlajamäki, A., *Chemical Engineering Journal*., **2021**, *407*, 126494.
14. Zhang, P.; He, M.; Huo, S.; Li, F.; Li, K., *Chemical Engineering Journal*., **2022**, *446*, 137081.
15. Barka, N.; Assabbane, A.; Nounah, A.; Laanab, L.; Ichou, Y. A., *Desalination*., **2009**, *235*(1-3), 264-275.
16. Li, L.; Wang, S.; Zhu, Z., *Journal of Colloid and Interface Science*., **2006**, *300*(1), 52-59.
17. Bhattacharyya, K. G.; Sen Gupta, S.; Sarma, G. K., *Applied Clay Science*., **2014**, *99*, 7-17.
18. Pathania, D.; Sharma, S.; Singh, P., *Arabian J. Chemistry*., **2017**, *10*, S1445-S1451.
19. Arora, D.; Arora, A.; Bala, R.; Panghal, V.; Kumar, S., *Water, Air, & Soil Pollution*., **2023**, *234*(8), 535.
20. Ahmaruzzaman, M. Progress in energy and combustion science, 2010, 36(3), 327-363.
21. Álvarez-Ayuso, E.; Querol, X.; Plana, F.; Alastuey, A.; Moreno, N.; Izquierdo, M.; Barra, M., *J. Hazardous Materi.,* **2008**, *154*(1-3), 175-183.
22. Niklio, I.; Markovi, S.; Jankovi–astvan, I.; Radmilovi, V. V.; Karanovi, L.; Babi, B.; Radmilovi, V. R., *Materials Letters*., **2016**, *176*, 301-305.

23. Zhang, M.; Zhao, M.; Zhang, G.; Mann, D.; Lumsden, K.; Tao, M., *Construction and Building Materials*., **2016**, *124*, 373-382.
24. Wang, Q.; Zeng, Y. E.; Wu, B. W., *Renewable and Sustainable Energy Reviews*., **2016**, *54*, 1563-1579.
25. Açı Iı, Ö.; Acar.; Khataee, A., *Chemosphere*., **2022**, *295*, 133870.
26. Darmayanti, L.; Kadja, G. T.; Notodarmojo, S.; Damanhuri, E.; Mukti, R. R., *Journal of Hazardous Materials*., **2019**, *377*, 305-314.
27. Yan, S.; Ren, X.; Zhang, F.; Huang, K.; Feng, X.; Xing, P., *Separation and Purification Technology*., **2022**, *284*, 120234.
28. El-Eswed, B. I.; Yousef, R. I.; Alshaaer, M.; Hamadneh, I.; Al-Gharabli, S. I.; Khalili, F., *International Journal of Mineral Processing*., **2015**, *137*, 34-42.
29. Suksiripattanapong, C.; Kua, T. A.; Arulrajah, A.; Maghool, F.; Horpibulsuk, S., *Construction and Building Materials*., **2017**, *146*, 312-320.
30. Zhou, W.; Lan, T.; Shang, G.; Li, J.; Geng, J., *J. Contaminant Hydrology*., **2023**, *255*, 104166.
31. Javadian, H.; Ghorbani, F.; Tayebi, H. A.; Asl, S. H., *Arabian J. of Chemistry*., **2015**, *8*(6), 837-849.
32. Singh, A.; Kumar, S.; Panghal, V., *Applied Water Science*., **2021**, *11*(9), 149.
33. Rice, E. W.; Bridgewater, L. Standard methods for the examination of water and wastewater., **2012**, *10*.
34. Yang, B.; Han, F.; Xie, Z.; Yang, Z.; Jiang, F.; Yang, S.; Li, Y., *RSC advances*., **2022**, *12*(27), 17147-17157.
35. Chen, K.; Lin, W. T.; Liu, W., *Advanced Powder Technology*., **2021**, *32*(8), 2929-2939.
36. Wu, B.; Wan, J.; Zhang, Y.; Pan, B.; Lo, I. M., *Environmental Science & Technology*., **2019**, *54*(1), 50-66.
37. Salam, M. A.; Mokhtar, M.; Albukhari, S. M.; Baamer, D. F.; Palmisano, L.; Al Hammadi, A. A.; Abukhadra, M. R., *Journal of Enviro. Management*., **2021**, *300*, 113723.
38. Mekonnen, D. T.; Alemayehu, E.; Lennartz, B., *Water*., **2020**, *12*(5), 1381.
39. Rashid, M.; Price, N. T.; Pinilla, M. Á. G.; O'Shea, K. E., *Water Res.,* **2017**, *123*, 353-360.
40. Lee, C.; Jung, J.; Pawar, R. R.; Kim, M.; Lee, S. M., *Journal of Industrial and Engineering Chemistry*., **2017**, *47*, 375-383.
41. Singh, A.; Arora, D.; Bala, R.; Khokhar, A.; Kumar, S., *Environmental Science and Pollution Research*., **2023**, 1-14.
42. Shah, K. H.; Fareed, M.; Waseem, M.; Shahida, S.; Hatshan, M. R.; Sarfraz, S.; Han, C., *Water*., **2023**, *15*(20), 3541.
43. Ajmal, Z.; Muhmood, A.; Usman, M.; Kizito, S.; Lu, J.; Dong, R.; Wu, S., *Journal of Colloid and Interface Science*., **2018**, *528*, 145-155.
44. Langmuir, I., *Journal of the American Chemical Society*., **1916**, *38*(11), 2221-2295.
45. Soni, H.; Padmaja, P., *Journal of Porous Materials*., **2014**, *21*, 275-284.
46. Freundlich, H. M. F., *J. Phys. Chem*., **1906**, *57*(385471), 1100-1107.
47. Temkin, M. J.; Pyzhev, V., *Acta Physico-Chimica Sinica*., **1940**, 217-222.
48. Foo, K. Y.; Hameed, B. H., *Chemical Engineering Journal*., **2010**, *156*(1), 2-10.
49. Lagergren, S., *Kungliga Svenska Vetenskapsakademiens Handlingar*., **1898**, *24*(4), 1-39.
50. Ho, Y. S., *Journal of Hazardous Materials*., **2006**, *136*(3), 681-689.
51. Weber Jr, W. J.; Morris, J. C., *Journal of the Sanitary Enginee. Division*., **1963**, *89*(2), 31-59.
52. Ngah, W. W.; Hanafiah, M. M., *Bioresource Technology*., **2008**, *99*(10), 3935-3948.
53. Wurtsbaugh, W. A., Paerl, H. W., & Dodds, W. K., *Wiley Interdisciplinary Reviews: Water*., **2019**, *6*(5), e1373.
54. Wang, S.L.; Cheng, C.Y.; Tzou, Y.M.; Liaw, R.B.; Chang, T.W.; J. H. Chen, J. H., *Journal of Hazardous Materials*., **2007**, *147*, 205–212.
55. Castaldi, P.; Silvetti, M.; Garau, G.; Deiana, S., *Journal of Hazardous Materials*., **2010**, *182*, 266–272.
56. Sreenivasulu, A.; Sundaram, E.; Reddy, M., *Indian J. Chem Technol.,* **1999**, *6*, 256–62.
57. Yang, Y.; Zhao, Y.; Babatunde, A.; Wang, L.; Ren, Y.; Han, Y., *Separation and Purification Technology.,* **2006**, *51*, 193–200.